


Cite this: *RSC Adv.*, 2018, 8, 35422Received 28th July 2018  
Accepted 10th October 2018

DOI: 10.1039/c8ra06358c

rsc.li/rsc-advances

# Self-calibrated optical thermometer based on luminescence from $\text{SrLu}_2\text{O}_4:\text{Bi}^{3+}, \text{Eu}^{3+}$ phosphors

Xueyan Chen, Zhigang Zheng, Liming Teng, Rongfei Wei, Fangfang Hu  
and Hai Guo \*

$\text{Bi}^{3+}, \text{Eu}^{3+}$  co-doped  $\text{SrLu}_2\text{O}_4$  phosphors were synthesized by a solid state reaction method. Their structural, luminescent and temperature sensing properties have been systematically investigated. The color-tunable emissions from violet to red were detected with the increase of  $\text{Eu}^{3+}$  concentration. Relying on energy transfer process from  $\text{Bi}^{3+}$  to  $\text{Eu}^{3+}$  and thermal quenching behaviour, the fluorescence intensity ratio (FIR) presents excellent temperature sensing performance. The maximum absolute and relative sensitivities reach  $1.10\% \text{ K}^{-1}$  and  $0.87\% \text{ K}^{-1}$ , respectively. These meaningful results indicate that  $\text{SrLu}_2\text{O}_4:\text{Bi}^{3+}, \text{Eu}^{3+}$  is a promising material for optical temperature sensing.

## Introduction

Recently, optical temperature sensors based on non-contact detection mode with rare earth (RE) ions doped luminescent materials have attracted extensive attention.<sup>1–8</sup> Commonly, temperature sensing optical parameters, such as emission intensity, luminescent lifetime and the fluorescence intensity ratio (FIR) have been widely adopted for their non-contact operating mode.<sup>5,9</sup> However, the measurement accuracy of temperature sensing strategy, which is based on the emission intensity, could be strongly affected by the external factors.<sup>10</sup> Optical thermometry based on FIR technique, by contrast, can reduce the dependence of measurement conditions and have obvious advantages, such as no requirement for contact, high sensitivity, rapid response, as well as high spatial and temperature resolutions.<sup>4</sup>

Therefore, searching for a FIR temperature sensing material, whose spectra display two discriminable peaks with different temperature-dependent luminescent behaviours, is an important way to develop optical thermometry.<sup>1</sup> In recent years, a series of FIR-based investigations have been systematically explored in order to search for high temperature sensitivity materials.<sup>4,6,11</sup> The typical conventional researches focus on the thermally coupled energy levels (TCEL) of RE ions, the relative sensitivities of which are difficult to promote due to their inherent energy gap.<sup>12,13</sup> Herein, a great many novel strategies and luminescent materials have been extensively investigated in order to promote relative sensitivity. According to the diverse thermal quenching behaviours of two intervalence charge transfer (IVCT) states, a novel thermometry strategy was proposed in 2016.<sup>1</sup> Another typical strategy

was based on the diversity in thermal behaviour of dual activators doped in separated matrixes.<sup>14</sup> Other kind of thermometry strategy was based on the phonon assisted energy transfer between RE ions (*e.g.*  $\text{Eu}^{3+}$  and  $\text{Tb}^{3+}$ ) doped in metal-organic framework.<sup>15</sup>

It is well known that RE ions doped luminescent materials are plentiful luminescent resources due to their abundant energy levels.<sup>16,17</sup>  $\text{Eu}^{3+}$  ion is a red activator originating from  $^5\text{D}_0\text{--}^7\text{F}_J$  ( $J = 0, 1, 2, 3, 4$ ) transitions under UV light excitation.<sup>17,18</sup>  $\text{Bi}^{3+}$  ion is another kind of activator, whose luminescence is attributed to the transition from  $6s^2$  to  $6s6p$  with broad absorption band in UV region.<sup>19,20</sup>  $\text{Bi}^{3+}$  ion can emit various wavelength including ultraviolet, blue, green, yellow and even red bands in different hosts.<sup>19</sup> These excellent luminescent properties make  $\text{Bi}^{3+}$  ion becomes a sensitizer to enhance  $\text{Eu}^{3+}$  emission in various hosts.<sup>16–22</sup>  $\text{Eu}^{3+}$  doped  $\text{SrLu}_2\text{O}_4$  and  $\text{SrGd}_2\text{O}_4$  have been considered as promising red phosphors in solid state lighting devices.<sup>23,24</sup> But energy transfer from  $\text{Bi}^{3+}$  to  $\text{Eu}^{3+}$  and temperature sensing property in  $\text{SrLu}_2\text{O}_4$  have never been investigated.

In this work, a series of  $\text{Bi}^{3+}, \text{Eu}^{3+}$  co-doped  $\text{SrLu}_2\text{O}_4$  phosphors were successfully synthesized by a solid state reaction method. The structural, luminescent and temperature sensing properties were investigated in detail. With the increase of  $\text{Eu}^{3+}$  content in  $\text{SrLu}_2\text{O}_4:0.005\text{Bi}^{3+}, y\text{Eu}^{3+}$ , tunable emission including violet, pink and red can be observed owing to energy transfer from  $\text{Bi}^{3+}$  to  $\text{Eu}^{3+}$ . Moreover, based on the opposite temperature dependence of  $\text{Bi}^{3+}$  and  $\text{Eu}^{3+}$  emission intensities, the temperature sensitivities reach high in the range from 315 to 543 K. More importantly, the main emission peak of  $\text{Eu}^{3+}$  and band of  $\text{Bi}^{3+}$  are well separated, providing an excellent signal discriminability for temperature sensing and detection.

Department of Physics, Zhejiang Normal University, Jinhua, Zhejiang, 321004, China.  
E-mail: ghh@zjnu.cn



## Experimental

A series of  $\text{SrLu}_{1.9}\text{O}_4:0.1\text{Eu}^{3+}$ ,  $\text{SrLu}_{2-x}\text{O}_4:x\text{Bi}^{3+}$  ( $x = 0, 0.25, 0.5, 1, 3\%$ ), and  $\text{SrLu}_{2-0.005-y}\text{O}_4:0.005\text{Bi}^{3+}, y\text{Eu}^{3+}$  ( $y = 0, 0.5, 2.5, 6, 10$  and  $12.5\%$ ) samples were prepared by conventional solid state reaction method. In this paper,  $\text{SrLu}_{1.9}\text{O}_4:0.1\text{Eu}^{3+}$ ,  $\text{SrLu}_{2-x}\text{O}_4:x\text{Bi}^{3+}$ , and  $\text{SrLu}_{2-0.005-y}\text{O}_4:0.005\text{Bi}^{3+}, y\text{Eu}^{3+}$  are briefly labelled as  $\text{SrLu}_2\text{O}_4:10\%\text{Eu}^{3+}$ ,  $\text{SrLu}_2\text{O}_4:x\text{Bi}^{3+}$ , and  $\text{SrLu}_2\text{O}_4:\text{Bi}^{3+}, y\text{Eu}^{3+}$ , respectively.  $\text{SrCO}_3$  (A.R.),  $\text{Bi}_2\text{O}_3$  (99.99%),  $\text{Lu}_2\text{O}_3$  (99.99%) and  $\text{Eu}_2\text{O}_3$  (99.99%) were used as starting materials. 2 wt%  $\text{NH}_4\text{Cl}$  (A.R.) was used as flux. The raw materials were mixed in an appropriate molar ratio and thoroughly grounded for 30 min in an agate mortar. The powder mixtures were put into crucibles and sintered at  $900^\circ\text{C}$  for 3 h in air. After repeated grinding, they were sintered at  $1300^\circ\text{C}$  for 10 h in air. The resulted samples were cooled down to room temperature and pulverized. Then the final products were gained for further characterization.

The crystalline structure of phosphors were investigated by X-ray diffraction (XRD) on a Rigaku MiniFlex/600 X-ray diffraction apparatus (Tokyo, Japan) with  $\text{CuK}\alpha$  ( $\lambda = 0.154056\text{ nm}$ ) radiation at 40 kV and 15 mA in a step size of  $0.02^\circ$ . The morphologies of samples were recorded by scanning electron microscope (Phenom ProX desktop SEM). The excitation and emission spectra were performed on an Edinburgh FS5

spectrofluorometer equipped with a continuous wave 150 W Xe lamp. Temperature-dependent luminescent spectra were measured using FS5 spectrofluorometer equipped with a TCB1402C temperature controller (China). Lifetime measurement was acquired on an Edinburgh FLS920 spectrofluorometer equipped with a nanosecond flashlamp (nF900) as excitation source. All measurements were performed at room temperature except temperature-dependent spectra.

## Results and discussion

Fig. 1(a) shows the XRD patterns of  $\text{SrLu}_2\text{O}_4:\text{Bi}^{3+}, 10\%\text{Eu}^{3+}$ ,  $\text{SrLu}_2\text{O}_4:10\%\text{Eu}^{3+}$  and  $\text{SrLu}_2\text{O}_4:0.5\%\text{Bi}^{3+}$  samples with  $\text{NH}_4\text{Cl}$  as flux, which can improve the crystallization, decrease the crystallization temperature and surface defect. Both  $\text{Bi}^{3+}$  ( $r = 1.03\text{ \AA}$ , CN = 6) and  $\text{Eu}^{3+}$  ( $r = 0.947\text{ \AA}$ , CN = 6) ions are suggested to occupy the sites of  $\text{Lu}^{3+}$  ( $r = 0.861\text{ \AA}$ , CN = 6) ion due to their similar radii and valence states. No trace of impure phase is observed when  $\text{Bi}^{3+}$  or  $\text{Eu}^{3+}$  ions are doped into this lattice. SEM image displayed in Fig. 1(b) exhibits that the synthesized  $\text{SrLu}_2\text{O}_4$  products are uniform with smooth facets, whose mean size is approximately  $10\text{ }\mu\text{m}$ .

Room-temperature photoluminescence emission ( $\lambda_{\text{ex}} = 327\text{ nm}$ ) and excitation ( $\lambda_{\text{em}} = 393\text{ nm}$ ) spectra of  $\text{SrLu}_2\text{O}_4:x\text{Bi}^{3+}$  phosphors are presented in Fig. 2(a) and (b), respectively.

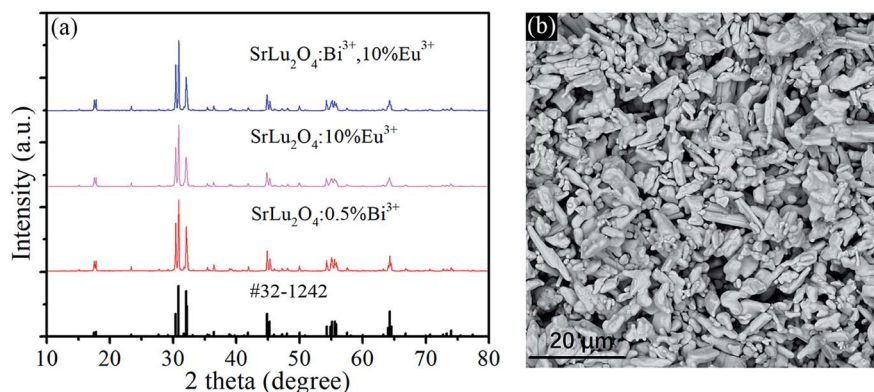


Fig. 1 (a) XRD patterns of  $\text{SrLu}_2\text{O}_4:\text{Bi}^{3+}, 10\%\text{Eu}^{3+}$ ,  $\text{SrLu}_2\text{O}_4:10\%\text{Eu}^{3+}$ ,  $\text{SrLu}_2\text{O}_4:0.5\%\text{Bi}^{3+}$ , and the standard data of  $\text{SrLu}_2\text{O}_4$  (JCPDS no. 32-1242) as a reference. (b) SEM micrograph of  $\text{SrLu}_2\text{O}_4:\text{Bi}^{3+}, 10\%\text{Eu}^{3+}$ .

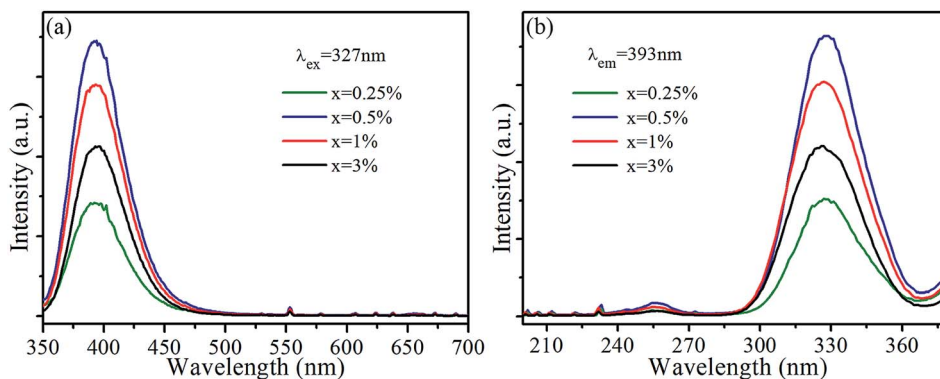


Fig. 2 (a) Emission ( $\lambda_{\text{ex}} = 327\text{ nm}$ ) and (b) excitation ( $\lambda_{\text{em}} = 393\text{ nm}$ ) spectra of  $\text{SrLu}_2\text{O}_4:x\text{Bi}^{3+}$  ( $x = 0, 0.25, 0.5, 1, 3\%$ ) samples.



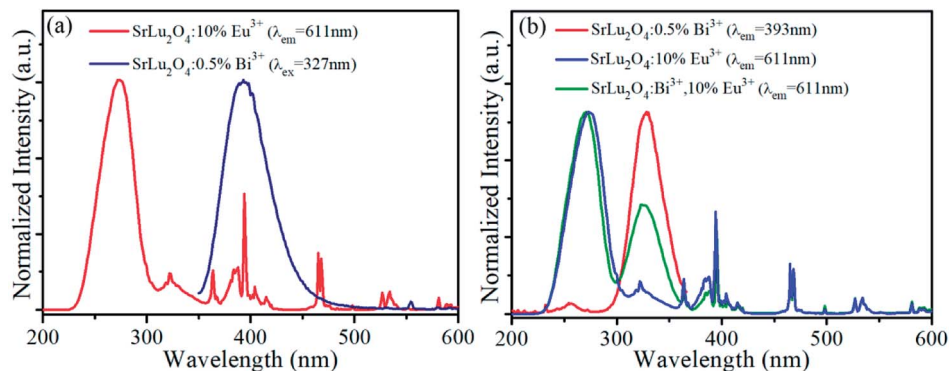


Fig. 3 (a) Spectra overlap between excitation ( $\lambda_{\text{em}} = 611 \text{ nm}$ ) of  $\text{SrLu}_2\text{O}_4:10\% \text{ Eu}^{3+}$  and emission ( $\lambda_{\text{ex}} = 327 \text{ nm}$ ) of  $\text{SrLu}_2\text{O}_4:0.5\% \text{ Bi}^{3+}$ . (b) Excitation ( $\lambda_{\text{em}} = 611 \text{ nm}$ ) spectra of  $\text{SrLu}_2\text{O}_4:10\% \text{ Eu}^{3+}$ ,  $\text{SrLu}_2\text{O}_4:\text{Bi}^{3+}, 10\% \text{ Eu}^{3+}$  and excitation ( $\lambda_{\text{em}} = 393 \text{ nm}$ ) spectra of  $\text{SrLu}_2\text{O}_4:0.5\% \text{ Bi}^{3+}$ .

Broadband blue emission from 350 to 510 nm with maximum at 393 nm is shown in emission spectra, which can be ascribed to the  $^3\text{P}_1 \rightarrow ^1\text{S}_0$  transition of  $\text{Bi}^{3+}$ .<sup>21</sup> In excitation spectra monitored at 393 nm, there is an excitation band ranging from 300 to 360 nm centered at 327 nm which can be attributed to the spin-allowed  $^1\text{S}_0 \rightarrow ^3\text{P}_1$  transition of  $\text{Bi}^{3+}$ .<sup>21</sup> With the increase of  $\text{Bi}^{3+}$  content, the emission and excitation intensities of  $\text{Bi}^{3+}$  increase sharply at first, reach the maximum at  $x = 0.5\%$ , and then remarkably decrease when  $\text{Bi}^{3+}$  content is further increased due to concentration quenching.

In order to explore energy transfer from  $\text{Bi}^{3+}$  to  $\text{Eu}^{3+}$  further, excitation spectra of  $\text{SrLu}_2\text{O}_4:10\% \text{ Eu}^{3+}$  ( $\lambda_{\text{em}} = 611 \text{ nm}$ ) and emission spectra of  $\text{SrLu}_2\text{O}_4:0.5\% \text{ Bi}^{3+}$  ( $\lambda_{\text{ex}} = 327 \text{ nm}$ ) are revealed in Fig. 3(a). In excitation spectra, there is a broadband from 230 to 305 nm centered at 274 nm, which can be ascribed to  $\text{Eu}^{3+}-\text{O}^{2-}$  charge transfer transition.<sup>25</sup> Due to  $^7\text{F}_0 \rightarrow ^5\text{D}_4, ^5\text{L}_7, ^5\text{L}_6, ^5\text{D}_2$  and  $^5\text{D}_1$  transitions of  $\text{Eu}^{3+}$  ion, several weak excitation peaks at 322, 364, 394, 465, 527 nm can be observed.<sup>19,21,25</sup> Meanwhile a broadband emission from 350 to 456 nm centered at 393 nm is presented in emission spectra ascribed to the  $^3\text{P}_1 \rightarrow ^1\text{S}_0$  transition of  $\text{Bi}^{3+}$  ion. It is obvious that there is an overlap between emission spectra of  $\text{Bi}^{3+}$  and excitation spectra of  $\text{Eu}^{3+}$ , indicating energy transfer process may occur from  $\text{Bi}^{3+}$  to  $\text{Eu}^{3+}$ .

Normalized excitation spectra of  $\text{SrLu}_2\text{O}_4:10\% \text{ Eu}^{3+}$ ,  $\text{SrLu}_2\text{O}_4:\text{Bi}^{3+}, 10\% \text{ Eu}^{3+}$  and  $\text{SrLu}_2\text{O}_4:0.5\% \text{ Bi}^{3+}$  phosphors are

displayed in Fig. 3(b). Excitation spectra of  $\text{SrLu}_2\text{O}_4:\text{Bi}^{3+}, 10\% \text{ Eu}^{3+}$  sample monitored  $\text{Eu}^{3+}$  emission ( $\lambda_{\text{em}} = 611 \text{ nm}$ ) ranging from 300 to 360 nm is almost similar with excitation spectra of  $\text{SrLu}_2\text{O}_4:0.5\% \text{ Bi}^{3+}$  sample monitored at 393 nm emission of  $\text{Bi}^{3+}$ . These phenomena from Fig. 3 imply that a portion of emission intensity of  $\text{Eu}^{3+}$  comes from energy transfer process from  $\text{Bi}^{3+}$  to  $\text{Eu}^{3+}$ .

On the other side, there is a band from 310 to 355 nm centered at 323 nm in excitation spectra of  $\text{SrLu}_2\text{O}_4:10\% \text{ Eu}^{3+}$ . That means characteristic excitation wavelength of  $\text{Bi}^{3+}$  ( $\lambda_{\text{ex}} = 327 \text{ nm}$ ) can also excite  $\text{Eu}^{3+}$  ion directly. To be specific, a competitive absorption exists between  $\text{Bi}^{3+}$  and  $\text{Eu}^{3+}$  ions in  $\text{SrLu}_2\text{O}_4:\text{Bi}^{3+}, 10\% \text{ Eu}^{3+}$ .

The emission spectra of  $\text{SrLu}_2\text{O}_4:\text{Bi}^{3+}, y\text{Eu}^{3+}$  ( $y = 0, 0.5, 2.5, 6, 10$  and  $12.5\%$ ) under 327 nm excitation are displayed in Fig. 4(a). As revealed in emission spectra, both emissions of  $\text{Bi}^{3+}$  and  $\text{Eu}^{3+}$  are observed. When the  $\text{Eu}^{3+}$  ion concentration increases, the red emission intensity increases rapidly and reaches the highest at 10%, after that the intensity decreases due to concentration quenching effect. However, the emission intensity from  $\text{Bi}^{3+}$  decreases slowly and monotonously with the increase of  $\text{Eu}^{3+}$  ion concentration. Therefore, conclusion can be drawn that the variation trend may owing to energy transfer from  $\text{Bi}^{3+}$  to  $\text{Eu}^{3+}$ .

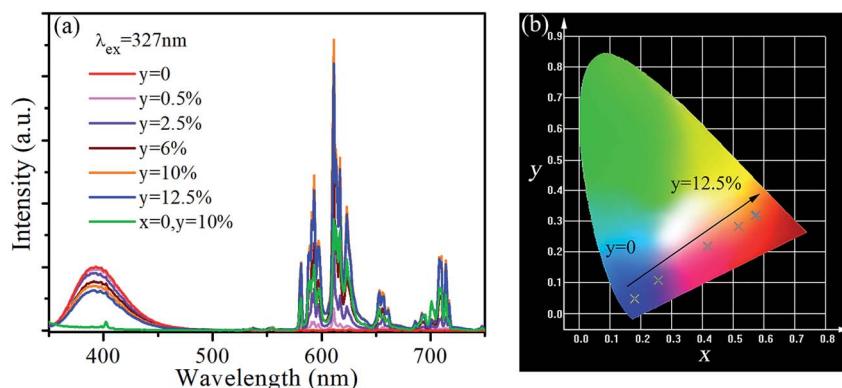


Fig. 4 (a) Emission spectra of  $\text{SrLu}_2\text{O}_4:\text{Bi}^{3+}, y\text{Eu}^{3+}$  ( $y = 0, 0.5, 2.5, 6, 10$  and  $12.5\%$ ) and  $\text{SrLu}_2\text{O}_4:10\% \text{ Eu}^{3+}$  under 327 nm excitation. (b) CIE chromaticity coordinates of  $\text{SrLu}_2\text{O}_4:\text{Bi}^{3+}, y\text{Eu}^{3+}$  ( $y = 0, 0.5, 2.5, 6, 10$  and  $12.5\%$ ) ( $\lambda_{\text{ex}} = 327 \text{ nm}$ ).



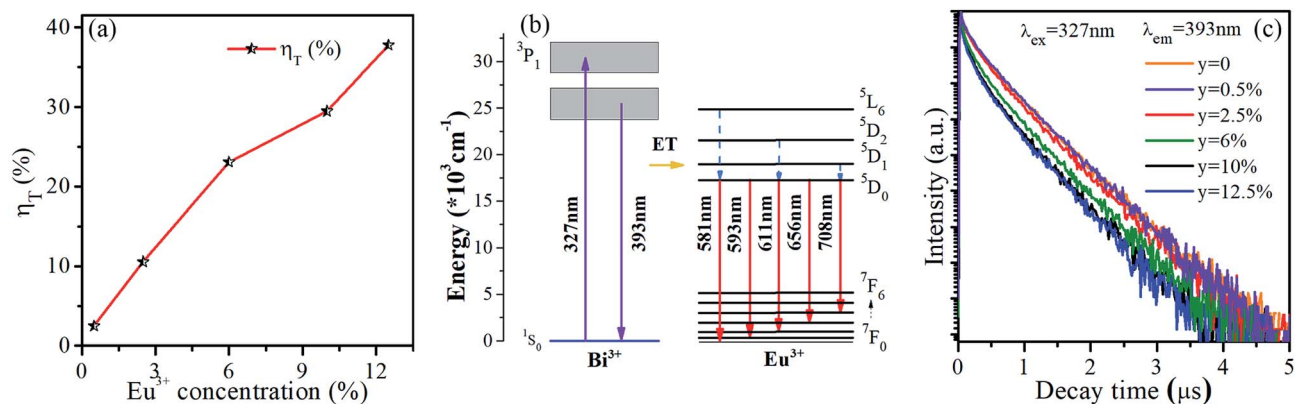


Fig. 5 (a) Energy transfer efficiency as a function of  $\text{Eu}^{3+}$  concentration. (b) The schematic energy-level diagram of  $\text{Bi}^{3+}$  and  $\text{Eu}^{3+}$  ions and energy transfer process. (c) Luminescence decay curves of  $\text{SrLu}_2\text{O}_4:\text{Bi}^{3+},y\text{Eu}^{3+}$  ( $y = 0, 0.5, 2.5, 6, 10$  and  $12.5\%$ ) ( $\lambda_{\text{ex}} = 327\text{ nm}$ ) monitored at 393 nm emission.

Fig. 4(b) gives the Commission International ed'Eclairage (CIE) chromaticity coordinates of  $\text{SrLu}_2\text{O}_4:\text{Bi}^{3+},y\text{Eu}^{3+}$  ( $y = 0, 0.5, 2.5, 6, 10$  and  $12.5\%$ ) phosphors under 327 nm excitation. The CIE chromaticity coordinates vary from (0.1805, 0.0478) to (0.5761, 0.3194) corresponding to  $y = 0$ –12.5%, locating in violet, pink and red regions. It is well-known that red and violet lights can promote photosynthesis effectively, which implies the  $\text{SrLu}_2\text{O}_4:\text{Bi}^{3+},\text{Eu}^{3+}$  phosphors may act as promising candidate to promote the photosynthesis of plant.<sup>26–28</sup>

The energy transfer efficiency from  $\text{Bi}^{3+}$  sensitizer to  $\text{Eu}^{3+}$  acceptor can be calculated by the following equation:<sup>5,25,29</sup>

$$\eta = 1 - I_s/I_{s0} \quad (1)$$

where  $\eta$  is the energy transfer efficiency,  $I_s$  and  $I_{s0}$  are the integrated intensities of  $\text{Bi}^{3+}$  with and without  $\text{Eu}^{3+}$  ion in  $\text{SrLu}_2\text{O}_4$  host, respectively. As displayed in Fig. 5(a), with the increase of  $\text{Eu}^{3+}$  ion concentration in  $\text{SrLu}_2\text{O}_4:\text{Bi}^{3+},y\text{Eu}^{3+}$  phosphors, the efficient energy transfer from  $\text{Bi}^{3+}$  to  $\text{Eu}^{3+}$  gradually

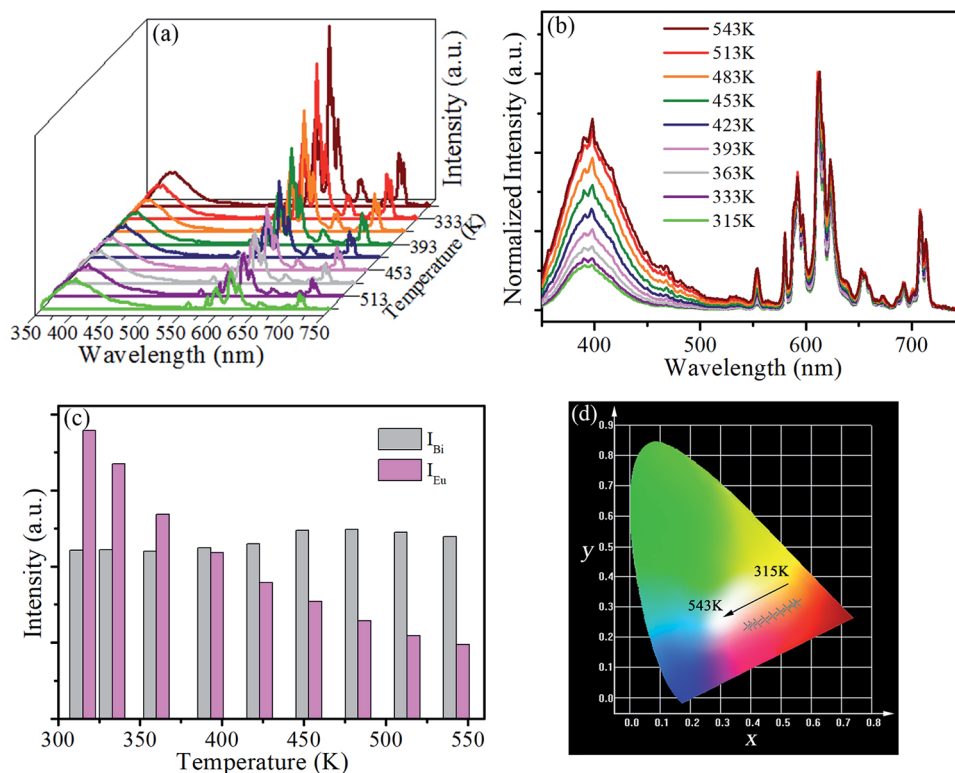


Fig. 6 (a) Temperature-dependent emission spectra of  $\text{SrLu}_2\text{O}_4:\text{Bi}^{3+},10\%\text{Eu}^{3+}$  sample recorded from 315 to 543 K. (b) The normalized emission spectra of  $\text{SrLu}_2\text{O}_4:\text{Bi}^{3+},10\%\text{Eu}^{3+}$  sample. (c) Temperature-dependent emission intensities of  $\text{Bi}^{3+}$  and  $\text{Eu}^{3+}$  ions at various temperatures. (d) CIE chromaticity coordinates of the emission color at various temperatures.





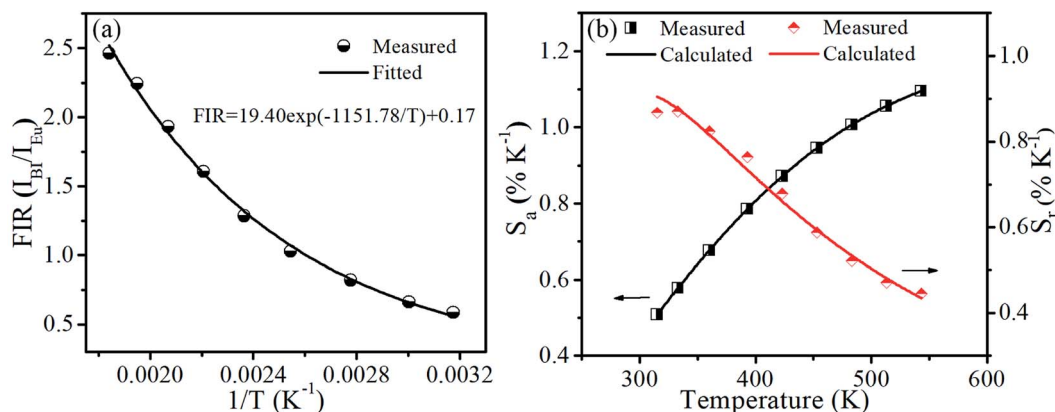


Fig. 7 (a) Experimental measured and fitted plots of FIR ( $I_{\text{Bi}}/I_{\text{Eu}}$ ) versus  $1/T$ . (b) Absolute sensitivity  $S_a$  and relative sensitivity  $S_r$  versus temperature.

Table 1 Optical parameters of several typical temperature sensing phosphor materials

Sensing materials	Temperature range (K)	$S_{a-\text{max}}$	$T_{\text{max}}$	Ref.
$\text{SrMoO}_4:\text{Er}^{3+}, \text{Yb}^{3+}$	93–773	0.0128	480	31
$\text{NaLuF}_4:\text{Yb}^{3+}, \text{Er}^{3+}, \text{Mn}^{2+}$	295–525	0.01099	295	6
$\text{ZnWO}_4:\text{Er}^{3+}, \text{Yb}^{3+}$	83–583	0.0099	583	2
$\text{YNbO}_4:\text{Er}^{3+}$	100–1600	0.0093	554	32
$\text{LuNbO}_4:\text{Mo}^{6+}, \text{Er}^{3+}$	323–673	0.0069	—	33
$\text{Gd}_2\text{O}_3:\text{Er}^{3+}, \text{Eu}^{3+}$	300–443	0.0043	300	34
$\text{Gd}_2\text{TiO}_5:\text{Yb}^{3+}, \text{Er}^{3+}$	298–573	0.004076	565	35
$\text{Y}_2\text{WO}_6:\text{Tm}^{3+}, \text{Yb}^{3+}$	303–473	0.0034	303	36
$\text{BaTiO}_3:\text{Er}^{3+}$	300–450	0.0032	400	37
$\text{SrLu}_2\text{O}_4:\text{Bi}^{3+}, \text{Eu}^{3+}$	315–543	0.0110	543	This work

increases and reaches maximum in the end concentration. However, the energy transfer efficiencies are all lower than 40% due to competitive absorption between  $\text{Bi}^{3+}$  and  $\text{Eu}^{3+}$  ions.

The luminescence decay curves of  $\text{Bi}^{3+}$  emission at 393 nm ( $\lambda_{\text{ex}} = 327$  nm) in all phosphors were displayed in Fig. 5(c). The average lifetime  $\tau$  can be evaluated by the following equation:<sup>4,29</sup>

$$\tau = \int tI(t)dt / \int I(t)dt \quad (2)$$

where  $I(t)$  is the emission intensity at time  $t$ . The lifetime  $\tau$  of  $\text{SrLu}_2\text{O}_4:\text{Bi}^{3+}, y\text{Eu}^{3+}$  ( $y = 0, 0.5, 2.5, 6, 10$  and  $12.5\%$ ) phosphors are 572, 569, 540, 494, 457 and 450 ns, respectively. It is obvious that the lifetime declines slightly with the increase of  $\text{Eu}^{3+}$  concentration, which illustrates the energy transfer from  $\text{Bi}^{3+}$  to  $\text{Eu}^{3+}$  is weak. Accordingly, more detailed investigation on energy transfer is inadaptable due to the competitive absorption between  $\text{Bi}^{3+}$  and  $\text{Eu}^{3+}$  ions.

Furthermore, temperature-dependent emission behaviour of  $\text{SrLu}_2\text{O}_4:\text{Bi}^{3+}, 10\% \text{Eu}^{3+}$  under 327 nm excitation has been systemically investigated in order to explore possible temperature sensing material. As displayed in Fig. 6(a), the  $\text{Eu}^{3+}$  emission intensity decreases rapidly, while the  $\text{Bi}^{3+}$  emission intensity increases slightly with an increase of temperature from 315 to 543 K. To better exhibit the relative emission intensities variation, luminescent spectra in the research

temperature range normalized to the 611 nm emission peak of  $\text{Eu}^{3+}$  is depicted in the Fig. 6(b).

The integrated intensities of  $\text{Bi}^{3+}$  and  $\text{Eu}^{3+}$ , as shown in Fig. 6(c), exhibit that the emission intensity of  $\text{Eu}^{3+}$  decreases greatly from 315 to 543 K. In contrast, the emission intensity of  $\text{Bi}^{3+}$  presents a slight rise. Such opposite temperature-dependent luminescent behaviour was adopted to investigate for the temperature sensing performance of  $\text{SrLu}_2\text{O}_4:\text{Bi}^{3+}, \text{Eu}^{3+}$  sample. Not surprisingly, the remarkable change in FIR ( $I_{\text{Bi}}/I_{\text{Eu}}$ ) results in the shift of emission color from red to pink as the CIE diagram displayed in Fig. 6(d).

According to the theory proposed by Struck and Fonger, the relationship between temperature and emission intensity can be expressed as:<sup>1</sup>

$$\frac{I(T)}{I_0} = \frac{1}{1 + A \exp(-\Delta E_a/k_B T)} \quad (3)$$

where  $I_0$  and  $k_B$  symbolize the emission intensity at 0 K and the Boltzmann constant, respectively.  $A$  is a constant. The quenching activate energy representing the distance from the bottom of the excitation state to the intersection between the excitation and ground states is denoted by  $\Delta E_a$ .

To further assess the temperature sensing performance of the  $\text{SrLu}_2\text{O}_4:\text{Bi}^{3+}, \text{Eu}^{3+}$  phosphor, the FIR ( $I_{\text{Bi}}/I_{\text{Eu}}$ ) of  $\text{Bi}^{3+}$  to  $\text{Eu}^{3+}$  can be deduced from eqn (3) and expressed as follows:<sup>30</sup>



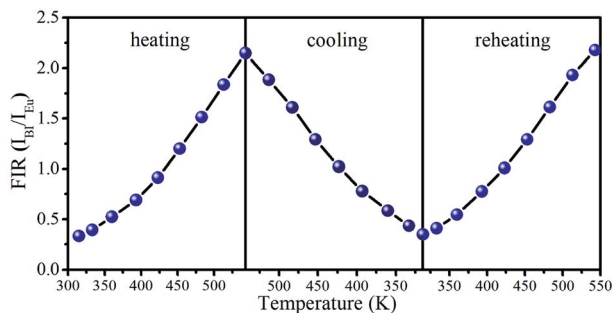


Fig. 8 Temperature-dependent FIR ( $I_{\text{Bi}}/I_{\text{Eu}}$ ) plots of in temperature cycling process from 315 to 543 K.

$$\text{FIR} = \frac{I_{\text{Bi}}}{I_{\text{Eu}}} = \frac{I_{0,\text{Bi}}}{I_{0,\text{Eu}}} \frac{1 + A_{\text{Eu}} \exp(-\Delta E_{\text{Eu}}/k_{\text{B}}T)}{1 + A_{\text{Bi}} \exp(-\Delta E_{\text{Bi}}/k_{\text{B}}T)} \approx B + C \exp(-\Delta E/k_{\text{B}}T) \quad (4)$$

where  $B$ ,  $C$  and  $\Delta E$  are the parameters related to  $\text{Bi}^{3+}$  and  $\text{Eu}^{3+}$ . The absolute sensitivity  $S_{\text{a}}$  and relative sensitivity  $S_{\text{r}}$  can be calculated and expressed as follows:<sup>5</sup>

$$S_{\text{a}} = \left| \frac{\partial \text{FIR}}{\partial T} \right| = C \exp(-\Delta E/k_{\text{B}}T) \times \frac{\Delta E}{k_{\text{B}}T^2} \quad (5)$$

$$S_{\text{r}} = 100\% \times \left| \frac{1}{\text{FIR}} \times \frac{\partial \text{FIR}}{\partial T} \right| = 100\% \times \frac{C \exp(-\Delta E/k_{\text{B}}T)}{B + C \exp(-\Delta E/k_{\text{B}}T)} \times \frac{\Delta E}{k_{\text{B}}T^2} \quad (6)$$

The plots of temperature-dependent FIR can be fitted by eqn (4) from 315 to 543 K, as shown in Fig. 7(a). Consequently, the values of  $B$ ,  $C$  and  $\Delta E$  parameters in this fitting function can be determined to be 0.17, 19.40 and 1151.78 K, respectively.

Fig. 7(b) presents the  $S_{\text{a}}$  and  $S_{\text{r}}$ , which were deduced by eqn (5) and (6), respectively. It is clear that absolute sensitivity  $S_{\text{a}}$  increases monotonously from 315 to 543 K, while the relative sensitivity  $S_{\text{r}}$  decreases with the rise of temperature. Noteworthy,  $\text{SrLu}_2\text{O}_4:\text{Bi}^{3+}, 10\% \text{Eu}^{3+}$  exhibits high temperature sensitivities with the maximal values of  $S_{\text{a}}$  and  $S_{\text{r}}$  are  $1.10\% \text{K}^{-1}$  and  $0.87\% \text{K}^{-1}$ , respectively. The obtained  $S_{\text{a-max}}$  is higher than most RE ions doped phosphor materials, as listed in Table 1.

In order to evaluate reversibility, the temperature-recycle measurements are studied in  $\text{SrLu}_2\text{O}_4:\text{Bi}^{3+}, 10\% \text{Eu}^{3+}$ . As revealed in Fig. 8, the sample has an excellent repeatability of the temperature-dependent FIR. The above results demonstrate that  $\text{SrLu}_2\text{O}_4:\text{Bi}^{3+}, \text{Eu}^{3+}$  phosphor is a promising material for optical temperature sensor.

## Conclusions

$\text{SrLu}_2\text{O}_4$  phosphors doped with different concentrations of  $\text{Bi}^{3+}$  and  $\text{Eu}^{3+}$  were successfully synthesized by solid state reaction method. The energy transfer from  $\text{Bi}^{3+}$  to  $\text{Eu}^{3+}$  was investigated by luminescent properties and decay curves. With the increase of the doped  $\text{Eu}^{3+}$  concentration, the color-tunable emissions

from violet to red were detected. Owing to the competitive absorption between  $\text{Bi}^{3+}$  and  $\text{Eu}^{3+}$  ions, the energy transfer efficiency from  $\text{Bi}^{3+}$  to  $\text{Eu}^{3+}$  is about 37.8%. Temperature-dependent emission behaviour of  $\text{SrLu}_2\text{O}_4:\text{Bi}^{3+}, 10\% \text{Eu}^{3+}$  under 327 nm excitation has been systemically investigated. Based on the opposite temperature dependence, the maximum absolute and relative sensitivities reach as high as  $1.10\% \text{K}^{-1}$  and  $0.87\% \text{K}^{-1}$ , respectively. The excellent temperature sensing performance indicates  $\text{SrLu}_2\text{O}_4:\text{Bi}^{3+}, 10\% \text{Eu}^{3+}$  is a promising candidate in the fields of optical temperature sensor.

## Conflicts of interest

The authors declare that there is no conflict of interests regarding the publication of this article.

## Acknowledgements

This work was supported by the National Natural Science Foundation of China 11374269 and 11465010.

## Notes and references

- Y. Gao, F. Huang, H. Lin, J. Zhou, J. Xu and Y. Wang, *Adv. Funct. Mater.*, 2016, **26**, 3139–3145.
- X. Chai, J. Li, X. Wang, Y. Li and X. Yao, *Opt. Express*, 2016, **24**, 22438–22447.
- J. Cao, X. Li, Z. Wang, Y. Wei, L. Chen and H. Guo, *Sens. Actuators, B*, 2016, **224**, 507–513.
- M. Ding, M. Xu and D. Chen, *J. Alloys Compd.*, 2017, **713**, 236–247.
- F. Huang and D. Chen, *J. Mater. Chem. C*, 2017, **5**, 5176–5182.
- H. Lu, H. Hao, H. Zhu, G. Shi, Q. Fan, Y. Song, Y. Wang and X. Zhang, *J. Alloys Compd.*, 2017, **728**, 971–975.
- W. Chen, J. Cao, F. Hu, R. Wei, L. Chen and H. Guo, *J. Alloys Compd.*, 2018, **735**, 2544–2550.
- S. Zhou, C. Duan and S. Han, *Dalton Trans.*, 2018, **47**, 1599–1603.
- Y. Cui, R. Song, J. Yu, M. Liu, Z. Wang, C. Wu, Y. Yang, Z. Wang, B. Chen and G. Qian, *Adv. Mater.*, 2015, **27**, 1420–1425.
- J. S. Zhong, D. Q. Chen, Y. Z. Peng, Y. D. Lu, X. Chen, X. Y. Li and Z. G. Ji, *J. Alloys Compd.*, 2018, **763**, 34–48.
- J. Cao, F. Hu, L. Chen, H. Guo, C. Duan and M. Yin, *J. Am. Ceram. Soc.*, 2017, **100**, 2108–2115.
- S. Zhou, X. Wei, X. Li, Y. Chen, C. Duan and M. Yin, *Sens. Actuators, B*, 2017, **246**, 352–357.
- W. J. Hu, F. F. Hu, X. Y. Li, H. W. Fang, L. Zhao, Y. H. Chen, C. K. Duan and M. Yin, *RSC Adv.*, 2016, **6**, 84610–84615.
- D. Q. Chen, M. Xu, S. Liu and X. Y. Li, *Sens. Actuators, B*, 2017, **246**, 756–760.
- A. M. Kaczmarek, Y. Y. Liu, C. H. Wang, B. Laforce, L. Vincze, P. Van Der Voort and R. Van Deun, *Dalton Trans.*, 2017, **46**, 12717–12723.
- K. Lenczewska, Y. Gerasymchuk, N. Vu, N. Q. Liem, G. Boulon and D. Hreniak, *J. Mater. Chem. C*, 2017, **5**, 3014–3023.



- 17 R. Cao, T. Fu, D. Peng, C. Cao, W. Ruan and X. Yu, *Spectrochim. Acta, Part A*, 2016, **169**, 192–196.
- 18 A. Escudero, C. Carrillo-Carrion, M. V. Zyuzin, S. Ashraf, R. Hartmann, N. O. Nunez, M. Ocana and W. J. Parak, *Nanoscale*, 2016, **8**, 12221–12236.
- 19 X. Y. Liu, H. Guo, S. X. Dai, M. Y. Peng and Q. Y. Zhang, *Opt. Mater. Express*, 2016, **6**, 3574–3585.
- 20 Y. C. Wang, J. Y. Ding, Y. Y. Li, L. F. Yang, X. Ding and Y. H. Wang, *RSC Adv.*, 2016, **6**, 42618–42626.
- 21 P. P. Dang, S. S. Liang, G. G. Li, Y. Wei, Z. Y. Cheng, H. Z. Lian, M. M. Shang, S. J. Ho and J. Lin, *J. Mater. Chem. C*, 2018, **6**, 6449–6459.
- 22 S. K. Hussain, L. K. Bharat, D. H. Kim and J. S. Yu, *J. Alloys Compd.*, 2017, **703**, 361–369.
- 23 L. Zhou, J. Shi and M. Gong, *Mater. Res. Bull.*, 2005, **40**, 1832–1838.
- 24 J. Singh and J. Manam, *J. Mater. Sci.*, 2016, **51**, 2886–2901.
- 25 K. Li, H. Lian, M. Shang and J. Lin, *Dalton Trans.*, 2015, **44**, 20542–20550.
- 26 D. Q. Chen, Z. Y. Wan, Y. Zhou, W. D. Xiang, J. S. Zhong, M. Y. Ding, H. Yua and Z. G. Ji, *J. Mater. Chem. C*, 2015, **3**, 3141–3149.
- 27 X. Y. Li, X. Chen, S. Yuan, S. Liu, C. Wang and D. Q. Chen, *J. Mater. Chem. C*, 2017, **5**, 10201–10210.
- 28 J. C. Zhang, X. G. Zhang, J. L. Zhang, W. T. Ma, X. Y. Ji, S. Z. Liao, Z. X. Qiu, W. L. Zhou, L. P. Yu and S. X. Lian, *J. Mater. Chem. C*, 2017, **5**, 12069–12076.
- 29 D. Xu, R. Wei, J. Cao and H. Guo, *Opt. Mater. Express*, 2017, **7**, 2899–2904.
- 30 H. Y. Lu, R. Meng, H. Y. Hao, Y. F. Bai, Y. C. Gao, Y. L. Song, Y. X. Wang and X. R. Zhang, *RSC Adv.*, 2016, **6**, S7667–S7671.
- 31 P. Du, L. H. Luo and J. S. Yu, *CURR. APPL. PHYS.*, 2015, **15**, 1576–1579.
- 32 X. Wang, X. P. Li, L. H. Cheng, S. Xu, J. S. Sun, J. S. Zhang, X. Z. Zhang, X. T. Yang and B. J. Chen, *RSC Adv.*, 2017, **7**, 23751–23758.
- 33 B. N. Tian, B. J. Chen, J. S. Sun, X. P. Li, J. S. Zhang and R. N. Hua, *Mater. Res. Express*, 2016, **3**, 5.
- 34 S. K. Ranjan, A. K. Soni and V. K. Rai, *Methods Appl. Fluoresc.*, 2017, **5**, 9.
- 35 J. S. Liao, Q. Wang, L. Y. Kong, Z. Q. Ming, Y. L. Wang, Y. Q. Li and L. X. Che, *Opt. Mater.*, 2018, **75**, 841–849.
- 36 A. K. Soni, *Mater. Res. Express*, 2018, **5**, 6.
- 37 D. K. Singh and J. Manam, *Ceram. Int.*, 2018, **44**, 10912–10920.

